15TH IEA HEAT PUMP CONFERENCE
MAY 26–29, 2026 | HOFBURG
VIENNA 2026
DECARBONISATION THROUGH INNOVATION

A one-dimensional approach to predict off-design performance of brazed plate evaporators in transcritical CO_2 heat pump applications

Seyed Mojtaba Hosseinnia[*a], Dominique Monney[b], Hakim Nesreddine[c], Sébastien Poncet[a]

[a]Department of Mechanical Engineering, Université de Sherbrooke, 2500 boulevard de l'Université, Sherbrooke, QC J1K 2R1, Canada
[b]Copeland, 145 Sherwood Dr, Brantford, ON, N3T 5S7, Canada
[c]Laboratoire des Technologies de l'énergie, Hydro-Québec, 600 Avenue de La Montagne, Shawinigan, QC, G9N 0C5, Canada

Abstract

A one-dimensional iterative model is developed to efficiently and accurately predict the thermal performance of a brazed plate heat exchanger (BPHX) evaporator in a transcritical CO_2 heat pump designed to meet the heating and cooling demands of a residential complex. The evaporator draws energy from a water-ethylene glycol (W-EG) solution, supplied via a stratified thermal energy storage tank at an inlet temperature of 15°C, while CO_2 evaporates at -1°C. The study aims to establish relationships among the overall pressure drops in both the CO_2 and W-EG channels, the W-EG outlet temperature, the CO_2 outlet condition (pressure, temperature, superheat degree, or quality), and variations in evaporator load for ±45% changes in the mass flow rate of each stream, reflecting seasonal building load fluctuations. The model applies continuity and energy equations at equidistant segments of the BPHX flow paths and incorporates state-of-the-art correlations for two-phase and single-phase heat transfer coefficients and pressure drop. It evaluates the off-design performance for a fixed plate configuration and dimensions. Results are presented as pressure drop profile, W-EG outlet temperatures, CO_2 outlet superheat or quality, and evaporator loads. The proposed model enables precise generation of performance maps for BPHX evaporators, advancing their optimization and integration in transcritical CO_2 heat pumps.

Keywords: Brazed plate heat exchanger; Transcritical CO2 heat pump; Thermal performance modeling; Two-phase flow;

1. Introduction

Brazed plate heat exchangers (BPHX) are compact thermal devices widely used in various heat transfer applications [1]. In addition to their roles in single-phase (SP) and supercritical heat exchange processes [2,3], they can also serve as two-phase (TP) heat exchangers, functioning as evaporators [4] and condensers [5]. The present work focuses on their application as an evaporator. Due to the intricate geometry of the flow passages formed by corrugated plates, a three-dimensional (3-D) numerical model becomes extremely computationally expensive and time-consuming, often requiring substantial simplifications such as assuming constant operating pressure or fixed boundary conditions. Furthermore, two-dimensional (2-D) models cannot accurately capture the complex geometrical configuration of the chevron plates, as no plane of symmetry can be identified under

* Corresponding author. Tel.: +1 819 821 8000 (ext. 62657)
E-mail address: seyed.mojtaba.hosseinnia@usherbrooke.ca

15th IEA Heat Pump Conference 2026 - ICO8.1 - https://doi.org/10.23697/30er-ax11

varying corrugation angles or plate orientations. Therefore, developing a reliable and computationally efficient one-dimensional (1-D) modeling approach is of particular interest.

When operating as an evaporator, the near-saturated liquid refrigerant enters the BPHX through the bottom inlet port at a known temperature, pressure, and mass flow rate, while the energy source (typically a water–glycol mixture, depending on the application) enters from the top inlet port with known thermodynamic conditions as well. For a given evaporator size, defined by a fixed number of plates and their geometric characteristics (length, width, thickness, corrugation angle, height, and pitch), the main design objective is to determine the outlet states on both sides. In practical applications, such as residential heating or cooling systems, the mass flow rate of each side may vary with changes in thermal load. However, as the short-term transient effects can be neglected, the system can be analyzed under a series of steady-state conditions, defining its off-design performance behavior.

Several modeling strategies have been proposed in the literature, though most assume that the outlet condition of one side is known a priori. For instance, Illan-Gomez et al. [6] developed a 1-D model for a BPHX evaporator assuming a predefined CO_2 outlet superheat. Similarly, Wu et al. [7] presented an algorithm that determines the corresponding lengths of the TP and superheating zones, again under the assumption of a known outlet state for one side. Jeong et al. [8] also proposed a 1-D model to calculate the outlet conditions of a BPHX evaporator for given inlet parameters on both the refrigerant and source sides, yet they introduced simplifications such as a fixed wall temperature on each side of the plate at each segments, an assumption that is not valid, particularly for stainless-steel plates with relatively low thermal conductivity.

In this study, a novel 1-D model is developed to iteratively determine the outlet conditions on both sides of the BPHX using only the known inlet states and geometric characteristics. The proposed algorithm is inspired by the iterative model previously developed by the authors for the design and off-design performance analysis of a BPHX operating as the gas cooler in a transcritical CO_2 heat pump system [9]. While the foundational structure of the method remains similar, the present work extends and modifies the algorithm to account for the TP heat transfer phenomena inherent to evaporator operation.

2. Methods and the proposed model

The proposed model in this study is based on a cell-by-cell 1-D approach. It means that the height of the plate is divided into fixed length segments (or cells), as it is illustrated in Figure 1, where the outlet of segment i is the inlet of segment $i+1$. The accuracy of the proposed approach strongly depends on the heat transfer coefficients (HTCs) selected for each zone of the exchanger. In contrast to the other 1-D models, like moving boundary models [10], here, the wall temperature at each side can be estimated. This advantage of the present proposed cell-by-cell approach allows implementations of complex heat transfer coefficients (local values) where the value of wall temperature, especially in the TP side, is needed. There are two iterative steps, in the segment level, and in the heat exchanger level. Figure 1 illustrates the algorithm of the proposed model in the segment level for both TP and SP. The steps will be repeated based on the convergence of the heat exchanger level.

The algorithm starts by guessing an outlet value for the refrigerant side (i.e., a superheat degree and an overall pressure drop), as it is depicted in Figure 2 for the *heat exchanger level* flowchart. Then, at the segmental level, the cells (i.e., segment) outlet conditions will be converged. Finally, the newly computed values of the last cell at the refrigerant side are compared with the initially guessed values, the guessed values will be corrected, and another round of the segment level iterations start. This loop continues until the error in the heat exchanger level is less than a predefined value for both temperature (ε_T) and pressure (ε_P), separately. The length of the segments is fixed. Depending on the temperature of the refrigerant (i.e., CO_2) at the local cell pressure, the cell in the refrigerant side can be in saturated boiling (SB), transition from SB to SP, or SP (i.e., superheating) zones. On the source side, it is always in single-phase liquid convection heat transfer. The pressure drop in the source side is negligible in comparison to the TP evaporation side. As depicted in the algorithm in Figure 2, there are two pairs of data in each cell. In TP cells the temperature and vapor quality $(x, P)_{TP}$ at inlet and outlet of cell are computed and stored. In SP cells, the temperature and pressure $(T, P)_{SP}$ at inlet and outlet of the cells will be computed and stored. In should be noted that in the water-ethylene glycol (EG) side, like the single-phase cells, just the temperature and pressures (at inlet and outlet of the cells) will be computed and stored.

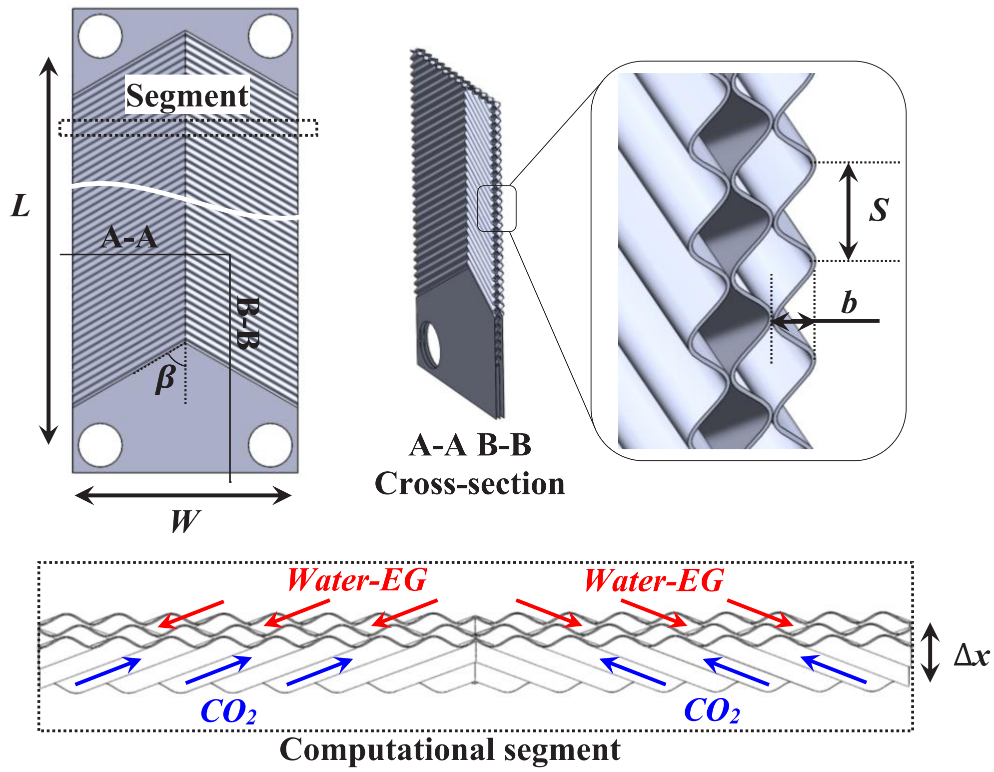

Figure 1. Brazed plate heat exchanger, the corresponding cross-section views, and the defined segment adapted from [9]

As mentioned earlier, the HTC of each zone is extremely important in the accuracy of the predicted values. Table 1 depicts the HTCs used in this model.

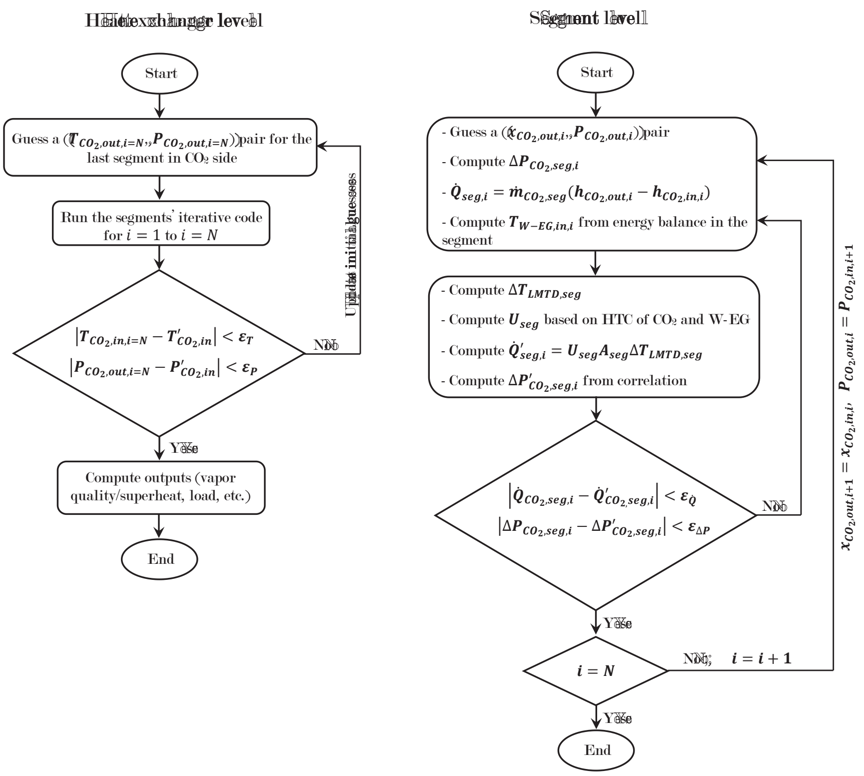

Figure 2. Iterative procedure for computing vapor quality (x) at the heat exchanger and the segment levels

Table 1: HTC of different zones

Working fluid	Two-phase	Single-phase
CO_2 [4]	$\max(h_{CO_2,cb}, h_{CO_2,nb})$ $h_{CO_2,cb} = 0.122(\frac{k_l}{D_h})Re_{eq}^{0.8}Pr_l^{0.333}$ $Re_{eq} = G\left[(1-x) + x(\frac{\rho_l}{\rho_g})^{0.5}\right]\frac{D_h}{\mu_l}$ $h_{CO_2,nb} = 0.58 \times h_0^* \times YY \times (\frac{k}{D_h})(\frac{PMR^{**}}{0.4})^{0.133}(\frac{q}{20})^{0.467}$ $YY = 1.2(\frac{P}{P_{crit}})^{0.27} + \frac{P}{P_{crit}}(2.5 + \frac{1}{1-\frac{P}{P_{crit}}})$ $q = h_{CO_2,nb}(T_{wall} - T_{sat})$	$0.277(\frac{k}{D_h})Re^{0.766}Pr^{0.333}$
W-EG***	$0.2302(\frac{k}{D_h})Re^{0.745}Pr^{0.4}$ [11]	

*h_0=4400 W m^{-2}K^{-1}, ** PMR = Plate mean roughness (in μm), *** Only single phase, P: segment pressure (kPa), P_{crit}: refrigerant critical pressure (kPa), T_{wall}: segment (refrigerant side) wall temperature (K), T_{sat}: Refrigerant local saturation temperature (at segment pressure) (K)

2.1. Wall temperature at each segment

It is worth nothing that the wall temperature at each side can be computed as follows:

$$T_{wall,W-EG,i} = T_{bulk,W-EG,i} - \frac{\dot{Q}_{seg,i}}{h_{W-EG,i}A_{seg}} \quad (1)$$

Where the heat transfer rate in the ith segment is $\dot{Q}_{seg,i}$ (W), $h_{W-EG,i}$ is the heat transfer coefficient of the W-EG side in ith segment (W K^{-1} m^{-2}), A_{seg} is the segment heat transfer area (m^2), $T_{bulk,W-EG,i}$ is the bulk temperature of the W-EG side (K) (average value of inlet and outlet in the segment in W-EG side), and finally $T_{wall,W-EG,i}$ is the wall temperature in the ith segment on the W-EG side.

The segment area is computed by taking into account the enlargement factor (φ) due to corrugation of the plates:

$$\varphi \approx \frac{1+\sqrt{1+Y^2}+4\sqrt{1+\frac{Y^2}{2}}}{6} \quad (2)$$

Where the Y is defined as $\pi b/S$. b and S are the corrugation amplitude and pitch as depicted in Figure 1. Hence the segment area is computed as $A_{seg} = \Delta x_{seg}\varphi W_{plate}$.

From the water-EG side wall temperature, and by knowing the fact that there is no source of energy embedded in the wall, the CO_2 side wall temperature can be estimated as:

$$T_{wall,CO_2,i} = T_{wall,W-EG,i} - \frac{\dot{Q}_{seg,i}\Delta x_{plate}}{k_{wall}A_{seg}} \quad (3)$$

Here, Δx_{plate} is the plate thickness (m), k_{wall} is the plate thermal conductivity (Wm^{-1}K^{-1}), and $T_{wall,CO_2,i}$ is the CO_2 side wall temperature (K).

2.2. Pressure drop

The two-phase frictional pressure drop can be computed by:

$$\Delta P_{tp,f} = f_{tp}2LG^2/(D_h\rho_{tp}) \quad (4)$$

Where G is the mass velocity (kg s^{-1}m^{-2}), L is the segment length (m), D_h is the hydraulic diameter of the segment (m). f_{tp} is the friction two-phase factor [12]:

$$f_{tp} = \frac{3.81\times10^{4}F_{Rf}}{Re_{tp}^{0.9}\left(\frac{\rho_l}{\rho_g}\right)^{0.16}} \qquad (5)$$

In this formula, $F_{Rf} = 0.183(\beta/30)^2 - 0.275(\beta/30) + 1.1$ (β is the corrugation angle), also, the two-phase Reynolds number is computed as $Re_{tp} = GD_h/\mu_{tp}$. ρ_l and ρ_g are saturated liquid and vapor densities at the segment pressure. For two-phase properties, this formula is used: $1/\rho_{tp} = x/\rho_g + (1-x)/\rho_l$, by computing the two-phase density at any average vapor quality, the other two-phase thermo-physical properties are computed by $\phi_{tp} = \rho_{tp}[x\phi_g/\rho_g + (1-x)\phi_l/\rho_l]$ (ϕ_{tp} can be viscosity, thermal conductivity, surface tension, etc.).

The single-phase frictional pressure drop is computed via Eq. (6):

$$\Delta P_{sp,f} = 2fLG^2/(\rho_{gas}D_h) \qquad (6)$$

The single-phase friction factor is estimated by:

$$f = \begin{Bmatrix} 26340 \times Re^{-0.83} & Re \le 550 \\ 570 \times Re^{-0.22} & Re > 550 \end{Bmatrix} \qquad (7)$$

Moreover, the gravitational pressure drop in the two-phase zone can be computed as:

$$\Delta P_{tp,g} = \rho_{tp} g \Delta z_{seg} \qquad (8)$$

Where the segment height and gravitational acceleration are included in this formula. Finally, the accelerational pressure drop, especially in two-phase zone, can be computed via:

$$\Delta P_{mom,tp} = \dot{m}_{ref}^2 \left\{\left[\frac{(1-x)^2}{\rho_L(1-\varepsilon)} + \frac{x^2}{\rho_G\varepsilon}\right]_{out} - \left[\frac{(1-x)^2}{\rho_L(1-\varepsilon)} + \frac{x^2}{\rho_G\varepsilon}\right]_{in}\right\} \qquad (9)$$

Regarding the void fraction (ε), the following correlation is used:

$$\varepsilon = \frac{x}{\rho_G}\left\{C_0\left[\frac{x}{\rho_G} + \frac{1-x}{\rho_L}\right] + \frac{1.18}{G_{ref}}\left[\frac{\sigma_{tp} g(\rho_L-\rho_G)}{\rho_L^2}\right]^{0.25}\right\}^{-1} \qquad (10)$$

C_0 is assumed $1 + 0.12(1+x)$ [13].

All numerical codes and functions are executed in MATLAB. The thermophysical properties of CO_2 are evaluated using the CoolProp library, which is accessed through Python links within the MATLAB [14] environment.

3. Results and discussion

First the accuracy of the proposed model and the errors in segments are presented. Then, the accuracy is discussed and evaluated against experimental data. In the next step, off-design performance of a given BPHX (the evaporator) is discussed.

3.1. Model accuracy

The length of the one pair of hot and cold channels is divided into axial segments of uniform height. In the present model, a minimum segment height of 0.01 m was adopted, corresponding to 600 segments along the effective heat-exchange length. A discretization sensitivity analysis was performed by reducing the segment height below 0.01 m, which resulted in variations of less than 0.5 % in the predicted results, indicating mesh-independent behavior. Conversely, increasing the segment height (e.g., to 0.1 m) led to increased numerical error and, in some cases, divergence of the segment-level iterative solution. Based on these observations, a segment height of 0.01 m was selected as an optimal compromise between numerical accuracy and computational cost.

As described in Section 2, the solution procedure is performed at the segment level. For each segment, two unknown variables must be iteratively guessed in order to simultaneously satisfy the energy balance and the pressure-drop equation. For segments operating in the two-phase region, these unknowns are the outlet vapor quality and the pressure drop. For segments operating in the single-phase region, the unknowns are the outlet temperature and the pressure drop. This procedure is repeated sequentially for all segments along the heat exchanger.

For each segment, only one combination of the two guessed variables satisfies both governing equations simultaneously. Since the residuals associated with the energy balance and pressure-drop equations are coupled, a normalized error is defined for each equation, and the sum of these normalized errors is minimized. The location of the minimum represents the converged solution for the corresponding segment.

The error contours presented in Figures 3 and 4 therefore represent numerical residuals associated with the iterative solution procedure, rather than convergence tolerance errors or deviations from experimental data. These contours are included to illustrate the existence of a unique solution and the robustness of the numerical approach.

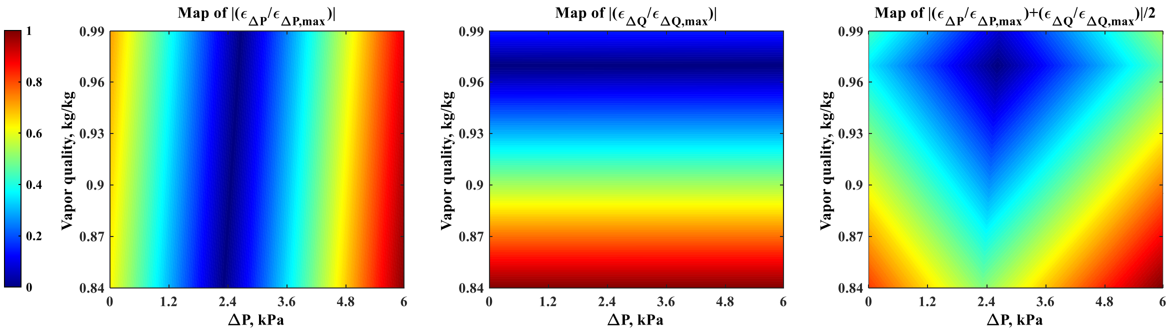

Figure 3. Error of an arbitrary segment of pressure drop, heat transfer value, and combined error

In single phase zone, temperature replaces the vapor quality, however, the concept is exactly the same. In other words, the minimum combined error only occurs in one combination of temperature and pressure, as illustrated in the right hand side graphs in Figure 4.

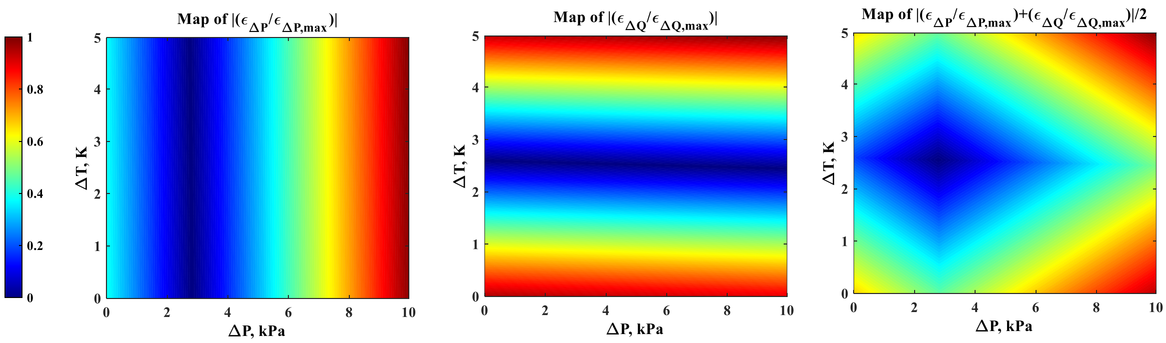

Figure 4. Error of an arbitrary segment in single phase (superheating) in pressure drop, heat transfer, and combined error

It should be noted that the minimization of the combined normalized residuals in each segment is also enforced in the transition segment, where the inlet lies in the two-phase zone while the outlet is located in single-phase zone.

To assess the accuracy of the proposed model, the predicted evaporator loads are compared against experimental data reported by Pardiñas et al. [15], as shown in Fig. 5. The BPHX used in the experimental study is manufactured by Alfa Laval (model AXP82) [16]. The heating source for CO_2 evaporation is greywater with inlet temperatures ranging from 20 °C to 30 °C at a constant mass flow rate of 0.31 kg s^{-1}. The evaporation pressure of CO_2 is varied from 3.5 MPa to 4.1 MPa, corresponding to saturation temperatures between 0.16 °C and 6.27 °C.

As the experimental study does not report CO_2 mass flow rates, an effective refrigerant mass flow rate is extracted from the measured water-side heat load and the refrigerant-side enthalpy rise. This inferred mass flow rate, together with the greywater operating conditions, is used as input to the proposed model. More details can be found in [15]. From the given experimental load, the CO_2 mass flow rates are computed and this value along with the greywater heat source data are the inputs of the proposed model presented in this study. The plates length and width are 320 mm and 120 mm, respectively. The effective values of the corrugation angle, pitch, and amplitude are estimated as 60°, 10 mm, and 3 mm, respectively, based on representative corrugated plate geometries commonly reported for brazed plate heat exchangers in the literature [17]. As shown in Figure 5, the predicted evaporator loads agree with the experimental data within ±10 % over the investigated operating range, indicating that the proposed model provides satisfactory accuracy for the intended application.

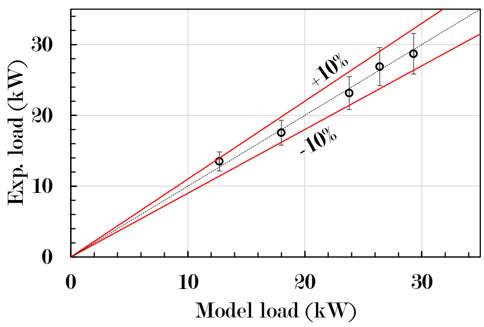

Figure 5. Comparing model predicted loads versus experimental data extracted from [15]

3.2. Off-design performance

The considered BPHX evaporator in this study has a width of 0.189 m, a length of 0.6 m, and consists of 60 plates. Each plate is made of stainless steel with a corrugation angle of 60°, a pitch of 6 mm, and an amplitude of 1.6 mm. Saturated liquid CO_2 enters the bottom port at −1 °C with mass flow rates of 0.0825 kg s^{-1}, 0.1444 kg s^{-1}, and 0.2063 kg s^{-1}, corresponding to different evaporator loads. The temperature distribution along the plate length and the associated vapor-quality variations are first analyzed, followed by a discussion of the pressure-drop profiles. The vapor superheat at the outlet is maintained constant by iteratively adjusting the mass flow rate of the water–ethylene glycol (W-EG) stream, which enters the top port at 15 °C.

3.2.1. Temperature profile

Figure 6 illustrates the results of the same BPHX at different evaporator loads. The mass flow rate of the refrigerants and W-EG are varied to have different loads. At the maximum load of 51.4 kW, CO_2 temperature falls down to −4°C due to the increased pressure drop in the two-phase zone. The temperature goes up to +4°C in the single-phase superheating zone at the top section of the evaporator, which respects the pre-determined 5 degree superheat value of the evaporator.

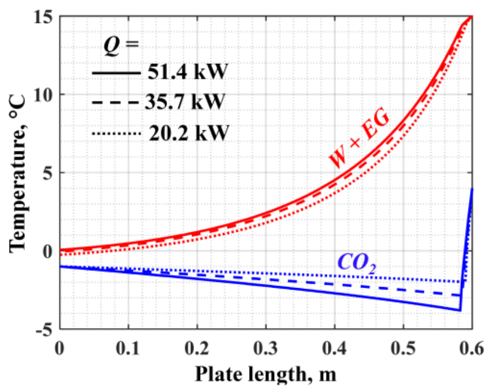

Figure 6. CO_2 temperature variations alongside of the plate height

The temperature profile exhibits similar behavior at lower mass flow rates; however, as the flow rate decreases, the two-phase pressure drop diminishes, leading to a smaller reduction in saturation temperature relative to the inlet condition of −1 °C. For instance, at a heating load of 20.2 kW, the minimum CO_2 temperature on the refrigerant side reaches −2 °C (only a 1 °C drop from the boundary condition). This trend clearly demonstrates the coupled thermal interaction and sensitivity of both fluid streams to variations in load, underscoring the BPHX's adaptability and efficiency under off-design operating conditions. Furthermore, Figure 7 presents the corresponding two-phase vapor quality evolution along the plate length. The vapor quality increases nonlinearly with height for all cases, reflecting the continuous phase transition of CO_2 from liquid to vapor throughout the flow path. Overall, these results highlight the strong dependence of CO_2 evaporation dynamics on the applied thermal load and provide valuable insight into the inherent flexibility and responsiveness of the BPHX during transient or variable-demand operation. A small length at top of the plate is responsible for the superheating of the saturated CO_2 vapor. This distribution has been observed in experimental thermography results performed by Navarro-Pris et al. [18] for BPHX working as evaporators.

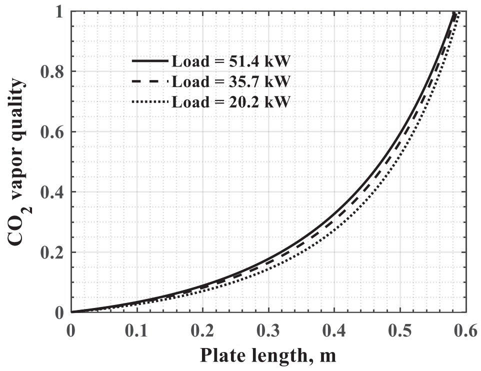

Figure 7. Vapor quality variations along the plate length at different evaporator loads

3.2.2. Pressure drop profile

The pressure profiles along side the plate wall are depicted in Figure 8. The figure illustrates the variation of pressure drop along the plate length of BPHX evaporator at different thermal loads. As shown, the pressure drop increases nonlinearly with the plate length and becomes more pronounced at higher loads due to the higher mass flux and vapor generation rate of CO_2. For the highest load (51.4 kW), the pressure drop reaches approximately 320 kPa at the outlet, indicating intensified frictional and accelerational losses associated with rapid vapor expansion and higher vapor quality. At lower loads (35.7 kW and 20.2 kW), the pressure drop is considerably smaller because of the reduced flow velocity and lower vapor content. The increasing curvature toward the outlet also reflects the dominance of the two-phase acceleration effect as evaporation progresses. Overall, this figure highlights the strong dependence of pressure drop on thermal load and vapor quality evolution, which is critical for the accurate design of BPHX evaporators to ensure stable operation and avoid excessive flow resistance under varying off-design conditions.

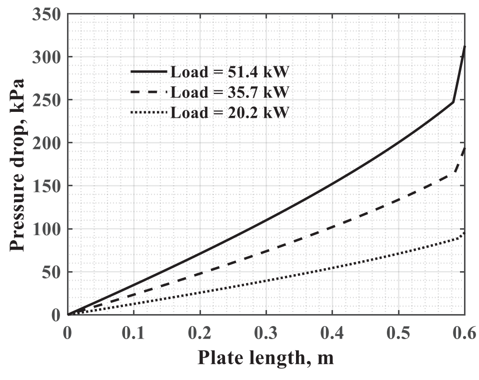

Figure 8. Pressure drop profile of CO_2 along the plate length

4. Conclusion

The developed one-dimensional iterative model accurately predicts the thermal–hydraulic behavior of a brazed plate heat exchanger operating as an evaporator in transcritical CO_2 heat pumps. It determines both outlet states directly from the inlet conditions while incorporating detailed local correlations for heat transfer and pressure drop. The model shows excellent agreement with experimental data, maintaining deviations within ±10% in predicted thermal load. In the off-design analysis, the CO_2 mass flow rate was varied by ±45%, while the outlet superheat was held constant through iterative adjustment of the water–glycol mass flow rate. Results indicate that the refrigerant-side pressure drop is highly sensitive to flow rate, increasing by approximately 2.3 times as the mass flow rises from 0.0825 kg s^{-1} to 0.2063 kg s^{-1} under the investigated conditions. Future work will focus on extending the model to two-dimensional flow distribution among channels, integrating condensation and dry-out detection, and coupling with system-level dynamic simulations for seasonal performance assessment. The flexibility of the proposed framework enables rapid generation of detailed performance maps, supporting both design optimization and control strategies. Overall, the model represents a robust and practical tool for the accurate analysis and optimization of CO_2 heat pumps employing brazed plate evaporators.

Acknowledgements

The authors acknowledge the financial support of the NSERC chair on industrial energy efficiency established in 2019 at Université de Sherbrooke and funded by Hydro-Québec (laboratoire des technologies de l’´energie), Natural Resources Canada (CanmetEnergy-Varennes) and Copeland.

References

[1] E. Mencke, A. Olsson, J. Larsson, A. Dahlquist, Y. Persson, P. Eriksson, Brazed plate heat exchangers and their applications, ASHRAE Trans. 111 (2005).
[2] S. Jain, A. Joshi, P.K. Bansal, A new approach to numerical simulation of small-sized plate heat exchangers with chevron plates, J. Heat Transf. 129 (2006) 291–297.
https://doi.org/10.1115/1.2430722
[3] K. Xu, R. Smith, Application of plate heat exchangers into heat exchanger networks retrofit with fixed structure, in: A.A. Kiss, E. Zondervan, R. Lakerveld, L. Özkan (Eds.), Comput. Aided Chem. Eng., Elsevier, 2019, pp. 505–510.
https://doi.org/10.1016/B978-0-12-818634-3.50085-0
[4] R.L. Amalfi, F. Vakili-Farahani, J.R. Thome, Flow boiling and frictional pressure gradients in plate heat exchangers. Part 1: Review and experimental database, Int. J. Refrig. 61 (2016) 166–184.
https://doi.org/10.1016/j.ijrefrig.2015.07.010
[5] X. Tao, C.A. Infante Ferreira, Heat transfer and frictional pressure drop during condensation in plate heat exchangers: Assessment of correlations and a new method, Int. J. Heat Mass Transf. 135 (2019) 996–1012.
https://doi.org/10.1016/j.ijheatmasstransfer.2019.01.132
[6] F. Illán-Gómez, J.R. García-Cascales, R. Molina-Valverde, F.J.S. Velasco, A discretization method for the characterization of a plate heat exchanger working as evaporator during transient conditions, Int. J. Therm. Sci. 184 (2023) 107998.
https://doi.org/10.1016/j.ijthermalsci.2022.107998
[7] W. Wu, H.M. Skye, J.J. Dyreby, Modeling and experiments for a CO_2 ground-source heat pump with subcritical and transcritical operation, Energy Convers. Manag. 243 (2021) 114420.
https://doi.org/10.1016/j.enconman.2021.114420
[8] H. Jeong, J. Oh, H. Lee, Experimental investigation of the performance of a plate heat exchanger as an organic Rankine cycle evaporator, Int. J. Heat Mass Transf. 159 (2020) 120158.
https://doi.org/10.1016/j.ijheatmasstransfer.2020.120158
[9] S.M. Hosseinnia, L. Amiri, H. Nesreddine, D. Monney, S. Poncet, An iterative approach for optimum sizing and off-design performance analysis of a water-cooled brazed plate heat exchanger as a supercritical CO_2 gas cooler, Int. J. Refrig. 180 (2025) 199–221.
https://doi.org/10.1016/j.ijrefrig.2025.08.021
[10] Y.-G. Chen, Q.-Y. Yang, A new moving-boundary algorithm to predict the heat transfer rate of a counter-flow water-cooled transcritical CO_2 gas cooler, Int. J. Refrig. 146 (2023) 357–365.
https://doi.org/10.1016/j.ijrefrig.2022.11.023
[11] A. Zendehboudi, Z. Ye, A. Hafner, T. Andresen, G. Skaugen, Heat transfer and pressure drop of supercritical CO_2 in brazed plate heat exchangers of the tri-partite gas cooler, Int. J. Heat Mass Transf. 178 (2021) 121641.
https://doi.org/10.1016/j.ijheatmasstransfer.2021.121641
[12] B. Thonon, Design method for plate evaporators and condensers, in: BHR Group Conf. Ser. Publ., Mech. Eng. Publ. Ltd., 1995, pp. 37–50.

[13] S. Buscher, Two-phase pressure drop and void fraction in a cross-corrugated plate heat exchanger channel: Impact of flow direction and gas-liquid distribution, Exp. Therm. Fluid Sci. 126 (2021) 110380. https://doi.org/10.1016/j.expthermflusci.2021.110380
[14] Á.Á. Pardiñas, H. Kauko, M.M. Hazarika, H. Selvnes, K. Banasiak, A. Hafner, Two-stage evaporator for R744 heat pumps using greywater as heat source, Energy Build. 289 (2023) 113047. https://doi.org/10.1016/j.enbuild.2023.113047
[15] Alfa Laval, AXP X-treme pressure brazed plate heat exchangers, available at: https://www.alfalaval.ca/products/heat-transfer/plate-heat-exchangers/brazed-plate-heat-exchangers/axp/ (accessed April 16, 2024).
[16] E. Navarro-Peris, L. Alvarez-Piñeiro, P. Albaladejo, L. Schnabel, J.M. Corberan, Refrigerant maldistribution in brazed plate heat exchanger evaporators. Part A: Testing campaign and experimental results, Int. J. Refrig. 131 (2021) 119–128. https://doi.org/10.1016/j.ijrefrig.2021.04.002